JACS
JOURNAL OF THE AMERICAN CHEMICAL SOCIETY
Communication
pubs.acs.org/JACS

In Situ Study of Fe_3Pt–Fe_2O_3 Core–Shell Nanoparticle Formation

Wen-I Liang,[†,‡] Xiaowei Zhang,[‡,§] Yunlong Zan,[∥] Ming Pan,[⊥] Cory Czarnik,[⊥] Karen Bustillo,[#] Jun Xu,[§] Ying-Hao Chu,[*,†,⊗] and Haimei Zheng[*,‡,▽]

[†]Department of Materials Science and Engineering, National Chiao Tung University, Hsinchu 300, Taiwan
[‡]Materials Science Division, Lawrence Berkeley National Laboratory, Berkeley, California 94720, United States
[§]National Laboratory of Solid State Microstructures, School of Electronic Science and Engineering and Collaborative Innovation Centre of Advanced Microstructures, Nanjing University, Nanjing 210093, China
[∥]School of Biomedical Engineering, Shanghai Jiao Tong University, Shanghai 200030, China
[⊥]Gatan, Inc., 5794 West Las Positas Boulevard, Pleasanton, California 94588, United States
[#]Molecular Foundry, Lawrence Berkeley National Laboratory, Berkeley, California 94720, United States
[⊗]Institute of Physics, Academia Sinica, Taipei 105, Taiwan
[▽]Department of Materials Science and Engineering, University of California, Berkeley, California 94720, United States

Supporting Information

ABSTRACT: We report an in situ study of Fe_3Pt-Fe_2O_3 core–shell nanoparticle growth using liquid cell transmission electron microscopy. By controlling the Fe-to-Pt ratio in the precursor solution, we achieved the growth of nanoparticles with the formation of an iron–platinum alloy core followed by an iron oxide shell in the electron beam-induced reactions. There was no substantial change in the growth kinetics of the iron oxide shell after the Fe–Pt alloy core stopped growing. The core growth was arrested by depletion of the Pt precursor. Heteroepitaxy of Fe_3Pt [101] (core)‖α-Fe_2O_3 [111] (shell) was observed in most of the nanoparticles, while a polycrystalline iron oxide shell is developed eventually for strain relaxation. Our studies suggest that Pt atoms catalyze the reduction of Fe ions to form the Fe_3Pt alloy core, and when Pt is depleted, a direct precipitation of iron oxide results in the core–shell nanostructure formation.

Platinum-containing nanoparticles with excellent electric, magnetic, and catalytic properties are important materials in energy, pharmaceutical, chemical, and electronic applications.[1] Over the past two decades, fine control over the size, shape, composition, and configuration of Pt-based nanomaterials has been achieved in colloidal synthesis. Among the various systems, the development of a core–shell nanoparticle has attracted a lot of interest since their biomedical,[2] magnetic,[2a,3] and catalytic[4] properties can be tailored using two disparate components.[5] Previously, core–shell Pt-CoO,[6] Pt-Fe_2O_3,[7] and FePt-Fe_3O_4 or FePt-$CoFe_2O_4$ nanoparticles[8] have been synthesized with tunable magnetic properties. FePd–iron oxide[9] nanoparticles have shown the potential to engineer the physical properties through surface modification. Figuerola et al. studied the formation of an FePt–iron oxide heterodimer from temperature-controlled experiments, and they proposed that FePt seeds catalyze iron oxide nucleation.[10] Liu et al. reported a two-step method: first, the FePt core nanoparticles grow as seeds, and second, an iron oxide sheath develops when there is no $Pt(acac)_2$ in the solution.[11] In spite of the great efforts, the formation mechanisms of Pt-based alloy-oxide systems are achieved mostly based on postreaction studies. There is little consensus concerning the fundamental questions on metal/metal-oxide core–shell nanoparticle formation. For instance, how does the metal/metal-oxide core–shell nanoparticle develop in the "one-pot" synthesis? What is the role of Pt in the formation of Fe–Pt alloy nanoparticles? In addition, the atomic structure of the interfaces between the metal or metal alloy and the metal oxide is still unclear.

Liquid cell transmission electron microscopy (TEM), which has enabled many studies of the growth kinetics of nanostructure formation in real time,[12] provides the opportunity for addressing the above questions. Here, we use the liquid cell TEM to study the formation of Fe_3Pt–Fe_2O_3 core–shell nanoparticles (see the Liquid cell development in previous publications[13]). By systematically changing the Fe:Pt ratio in the precursor solution, the structure, composition, and morphology of nanoparticles are investigated. With the high sensitivity and high spatial and temporal resolution advanced imaging and spectroscopy, the unique growth pathways for FePt–FeO_x core–shell nanoparticle formation have been revealed. Key questions regarding the core–shell particle growth, the role of Pt, and the interfaces have been addressed.

The growth solution was prepared by dissolving $Pt(acac)_2$ and $Fe(acac)_3$ in benzyl ether in the presence of oleylamine and oleic acid, which acted as both solvent and surfactant.[11,14] We loaded 100 nL of growth solution into a liquid cell by capillary force, which formed a thin liquid layer (~100 nm) sandwiched between two silicon nitride membranes (Figure S1). Different precursor ratios, Fe:Pt = 1:2, 1:1, and 4:1, were used to investigate the formation of nanoparticles. The in situ TEM studies were performed using a JEOL 3010 TEM operated at 300 kV, a FEI F20 Tecnai operated at 200 kV equipped with a K2 IS camera, and TitanX with a Bruker Quantax energy-dispersive X-ray

Received: September 24, 2015
Published: November 13, 2015

DOI: 10.1021/jacs.5b10076
J. Am. Chem. Soc. 2015, 137, 14850–14853

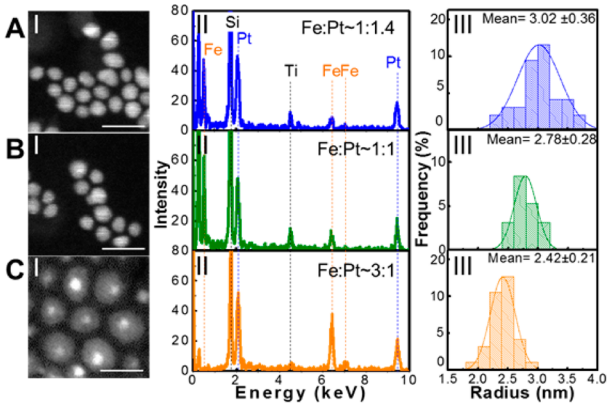

Figure 1. (I) HAADF images of as-grown Fe−Pt nanoparticles, (II) corresponding EDS spectra for composition analysis, and (III) nanoparticle size distributions for sample precursor concentration ratios Fe:Pt = 1:2 (A), 1:1 (B), and 4:1 (C). The measured nanoparticle composition ratio from EDS is indicated in panel II. Scale bars are 20 nm.

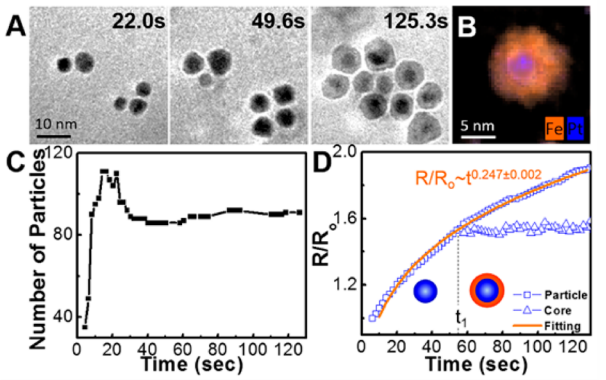

Figure 2. Growth trajectory of nanoparticles. (A) Sequential images captured during growth of Fe:Pt = 4:1 solution, showing core−shell structure. (B) EDS mapping of one core−shell nanoparticle. Blue represents Pt, and orange is for Fe. Original maps are in the SI. (C) Plot of particle numbers as a function of time. (D) Trace for growth kinetics.

spectrometry (EDS) detector. An electron beam current density at (5−9) × 10^4 A/m^2 was maintained through the study. Detailed descriptions of solution preparation, liquid cell preparation, and imaging conditions can be found in the Supporting Information (SI).

Figure 1 shows the representative sequential images of nanoparticles synthesized in a liquid cell with three different ratios of $Fe(acac)_3$ to $Pt(acac)_2$ in the precursor solution (also see SI movies for Fe:Pt = 1:2 (Movie S1), 1:1 (Movie S2), and 4:1 (Movie S3). The high-angle annular dark-field imaging in scanning transmission electron microscopy (HAADF-STEM) shows that nanoparticles have different morphology when synthesized in a precursor solution with different Fe:Pt ratio (panel I). The nanoparticle composition is quantified using EDS (panel II). It shows the corresponding characteristic X-ray peaks as indicated by the blue dashed line for Pt L-edge and the orange dashed line for Fe K-edge. The elemental ratio of Fe:Pt can be estimated by integrating the area under the Kα and Kβ peaks of the Fe edge and the Lα and Lβ of the Pt edge, and using Cliff−Lorimer *k*-factors to calculate the composition. The composition of the as-grown nanoparticles in the Fe:Pt = 1:2 solution (Figure 1A) shows both Pt and Fe. The elemental ratio of Fe:Pt is estimated as 1:1.4. The size distribution of FePt nanoparticles (panel III) shows an average size of 3.0 nm. Figure 1B shows the results for the nanoparticles grown in Fe:Pt = 1:1 solution. The nanoparticle sizes are smaller with an average diameter of 2.8 nm. The nanoparticles are composed of Pt and Fe with almost equal ratio. With the Fe precursor concentration of Fe:Pt = 4:1, a core−shell structure is formed (Figure 1C). In a HAADF-STEM image, the contrast can be attributed largely to the atomic number *Z*, the bright-core nanoparticle implying Pt abundance and light shell suggesting Pt deficiency. The composition of the nanoparticle core is also identified in the EDS spectrum,roughly Fe:Pt = 3:1 ratio. In addition, an average core diameter is 2.4 nm. Through these systematic investigations, we conclude that the Pt−Fe alloy nanoparticle size decreases with decreasing Pt precursor concentration, implying that the growth of nanoparticle size correlates with Pt precursor concentration. Also, when the Fe precursor concentration is high (at least 4 times higher than that of the Pt precursor), the morphology of a nanoparticle transforms from a simple nanoparticle to a core−shell heterostructure.

Figure 2 shows the growth and kinetic analysis of core−shell heterostructures in the Fe:Pt = 4:1 solution. Based on the fact that the iron oxide has a relatively light contrast compared to the Fe−Pt alloy, time sequential images show that the nanocrystal forms Fe−Pt alloy first and then Fe-rich composite shell at a later stage. An EDS map has been obtained to further identify the core and shell distribution. The EDS map overlaying the Pt L-edge signal (blue) and Fe K-edge signal (orange) is shown for clarity (Figure 2B). The presence of Pt in the core region while the Fe signal covers the entire particle is achieved. Quantification of the two different regions results in an Fe:Pt ratio in the particle core of 3.5:1, and an Fe:O ratio in the particle shell of 1:1.6; details can be found in Figure S3A,B. Additionally, the elemental profile of a nanoparticle is shown in Figure S3C. From these plots, we have found that oxygen is deficient at the core region (~3 nm in the middle of plot) where Pt is rich, and the Fe signal covers the whole particle, indicating the particle configuration of core−shell. Figure 2C plots the number of particles observed within the viewing window area (~150 × 150 nm^2) as a function of time. An initial outburst followed by coalescence and growth suggests a common growth behavior in colloidal synthesis. The nanoparticle growth can be described as monomer attachment and coalescence behavior (see Figure S5). The growth trajectory (Figure 2D) shows a continuous growth for the overall particle size, where the growth of the nanoparticle core ceases when the sheath starts developing (at time = t_1). Generally, the kinetics of particle growth follows the formula $r/r_o \sim t^{\beta}$, where *r* is the radius of nanoparticle, r_o is the critical radius of nuclei, and β is the growth exponent. The growth exponent is calculated to be 0.25, falling in the region of diffusion-limited growth of the Lifshitz−Slyozov−Wagner model.[15] This growth exponent is consistent with other reports of nanoparticle growth in the TEM liquid cell.[16] The continuous growth curve suggests that the particle formation undergoes an uninterrupted precipitation process with low or no energy barrier for shell growth on the core. Most nanoparticles grow into core−shell structures, indicating that the heterogeneous nucleation is more favorable.

We track the structural evolution during core−shell growth using high spatial and temporal resolution TEM. Sequential TEM images from different nanoparticles are displayed in Figure 3. Corresponding fast Fourier transform (FFT) and inverse fast Fourier transform (IFFT) are shown respectively for structure identification. Figure 3A shows images extracted from Movie S4.

DOI: 10.1021/jacs.5b10076
J. Am. Chem. Soc. 2015, 137, 14850−14853

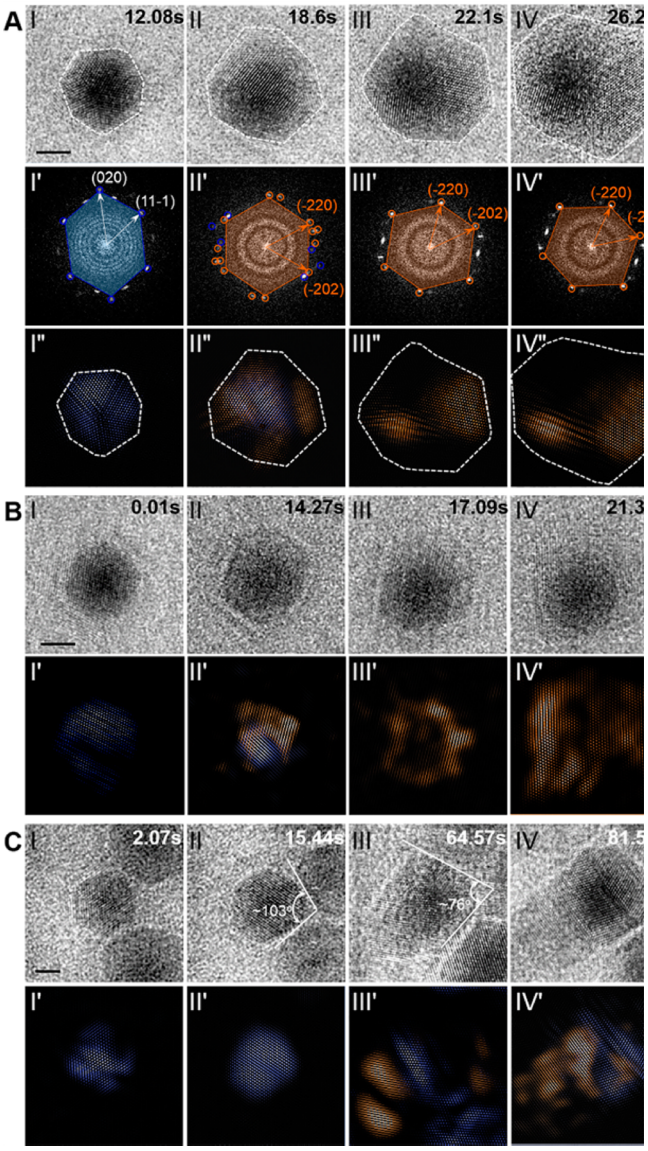

Figure 3. Structural evolution during growth. (A) Core−shell structure formation with a multitwined Fe_3Pt alloy: panels I−IV, in situ HRTEM captured as a function of time; I′−IV′, corresponding fast Fourier transform (FFT) of the HRTEM images; and I″−IV″, corresponding inverse fast Fourier transform (IFFT) of the HRTEM images. Blue represents the core nanoparticle, and orange represents the sheath. (B) Growth of untwined Fe_3Pt alloy: panels I−IV, in situ HRTEM images; I′−IV′, corresponding IFFT images. (C) asymmetric growth of the nanoparticle: panels I−IV, sequential HRTEM images; I′−IV′, corresponding IFFT images showing the asymmetric sheath distribution. Blue highlights the Fe_3Pt structure, and orange indicates the α-Fe_2O_3 structure-related information. Scale bars are 2 nm.

At the early stage of growth (0−15 s), the particle rotates vigorously, and it resides along the Fe_3Pt [101] viewing zone axis with cubic structure. One set of Bragg diffraction spots representing the [101] viewing zone axis is highlighted by the blue hexagon. A twinned structure is clearly found in the Fe−Pt alloy; the detailed structure analysis of a nanoparticle with (111) twinning is shown in the SI and Figure S7. During the subsequent period of time (15−20 s), a light contrast shell develops (Figure 3A-II). A direct heterogeneous nucleation and crystallization of iron oxide is observed, in accordance with classical theory.[17] From the corresponding FFT in Figure 3A-II′, we can identify several sets of Bragg diffraction spots belong to Fe_3Pt with [101] zone axis (in blue circle) while others belong to α-Fe_2O_3 (in orange circle), also see Figure S8. The Fe_3Pt particle in Figure 3A(II) is off-axis due to the rotation. An orange hexagon is selected for display and is identified as the α-Fe_2O_3 [111] (rhombohedral) viewing axis. The epitaxial relation was assigned where $(020)_{Fe_3Pt}$ associates with $(\bar{2}20)_{\alpha\text{-}Fe_2O_3}$ and $(11\bar{1})_{Fe_3Pt}$ associates with $(\bar{2}02)_{\alpha\text{-}Fe_2O_3}$. The lattice mismatch between the two lattices is calculated according to the formula $|d_{shell} - d_{core}|/d_{core}$; they are 12.3% and 6.7%, respectively. Figure 3A-II″ shows blue and orange IFFTs indicating the structure distribution of core−shell nanoparticles in panel II. In the late stage of growth (after 20 s), the growing iron oxide layer covers the whole Fe_3Pt core particle and the α-Fe_2O_3 [111] zone axis dominates (Figure 3A-III,IV and their corresponding FFT).

Analysis of another particle without twinned structure is shown in Figure 3B. The growth morphology is similar while the shell grows geometrically in a nonconcentric fashion. Several factors may contribute the growth fluctuations including epitaxial strain, geometric limitation confined by adjacent nanoparticles, the local inhomogeneous absorption of molecules or impurities on the nanoparticle surface, and local precursor concentration variations. The geometric effect is shown in Figure 3C. At the early stage of growth (less than 15 s), the nanoparticle is blocked by two adjacent nanoparticles. The growth direction is limited to roughly 103° as indicated in Figure 3C-II. When the sheath starts developing, another adjacent nanoparticle corners and reduces the growth direction to roughly 76°, as seen in Figure 3C-III. Finally, the heterostructure forms as a peanut shape with an Fe−Pt nanoparticle on one side and an iron oxide component on the other side (Figure 3C-IV,IV′).

Figure 4 shows the interfaces of core−shell structure, which are captured during the middle stage of growth. Two types of interfaces between Fe−Pt alloy and the iron oxide are identified: one with a coherent interface (Figure 4A) and another with dislocation formed in the iron oxide shell (Figure 4B). The

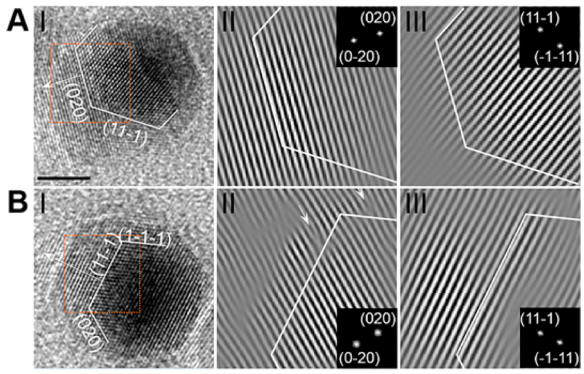

Figure 4. Interface structure of core−shell nanoparticles. (A) Interface at (020) plane of Fe_3Pt: panel I, HRTEM images of interface with growth direction along [020]; II, IFFT images of the interfacial region (orange box in I) using Fourier spatial frequency corresponding to (020) plane (inset); and III, IFFT images using Fourier spatial frequency corresponding to $(11\bar{1})$ plane (inset). (B) Interface at $(11\bar{1})$ plane: panel I, HRTEM image of interface with growth direction along $[11\bar{1}]$; II, IFFT image of the square region (orange box in I) using Fourier spatial frequency corresponding to (020) plane (inset), with dislocation indicated by white arrow; III, IFFT image using Fourier spatial frequency corresponding to $(11\bar{1})$ plane (inset). Scale bars are 2 nm.

DOI: 10.1021/jacs.5b10076
J. Am. Chem. Soc. 2015, 137, 14850−14853

Scheme 1. Schematic Illustration of the Formation Pathway of Fe_3Pt–Fe_2O_3 Core–Shell Heterostructure[a]

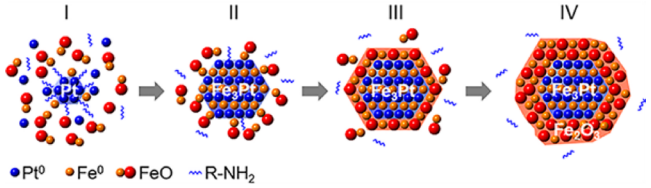

[a]The study of nanoparticle growth trajectories in situ and the revelation of Fe_3Pt–Fe_2O_3 core–shell nanoparticle evolution contribute to the understanding of solution-based synthesis and enriching the field of nanomaterials engineering.

dislocation formation is likely due to strain relaxation (see more in SI).

Based on the in situ observation, we propose a pathway of the Fe_3Pt–Fe_2O_3 core–shell nanoparticle formation as shown in Scheme 1. Pt ion can be easily reduced to metal under the electron beam due to the higher redox potential than that of $Fe(acac)_3$ as well as the lower decomposition temperature.[18] Once Pt nanoparticles nucleate, oleylamine ligands ($R\text{-}NH_2$) prefer to bind with Pt (Stage I) surface.[19] Since Pt catalyzes the electron transfer between oleylamine and Fe ions,[18a,b] the reduction of iron ($Fe^{3+}\rightarrow Fe^0$) and formation of Pt–Fe alloy nanoparticle can be achieved. The Fe^{3+} ions can be reduced on the Pt nanoparticle surface, and they rearrange to form Fe_3Pt.[18a] The core size is defined when Pt is depleted in the precursor solution, where the reduction of Fe is diminished (Stage II). As a consequence, the absorbed Fe ions on the nanoparticle surface develop into iron oxide without further reduction (Stage III). In order to compensate the large lattice mismatch between Fe_3Pt and α-Fe_2O_3, a polycrystalline shell is expected from strain relaxation (Stage VI).

■ ASSOCIATED CONTENT

Supporting Information

The Supporting Information is available free of charge on the ACS Publications website at DOI: 10.1021/jacs.5b10076.

Material and methods; liquid cell fabrication; details of TEM characterization, imaging conditions, and post-process; growth images of Fe:Pt = 1:1 and 1:2 solution; original EDS maps; the coalescence behavior; analysis of Fe_3Pt and α-Fe_2O_3 structure; detailed analysis for Figure 3A-II and raw images for Figure 3; two comparison tables with related parameters (PDF)

Movie S1: growth of NPs in Fe:Pt = 1:2 solution (AVI)

Movie S2: growth of NPs in Fe:Pt = 1:1 solution (AVI)

Movie S3: growth of NPs in Fe:Pt = 4:1 solution (AVI)

Movie S4: drift-corrected growth of NPs in Fe:Pt = 4:1 solution, recorded using K2 IS detector, in real time (AVI)

■ AUTHOR INFORMATION

Corresponding Authors

*yhc@nctu.edu.tw

*hmzheng@lbl.gov

Notes

The authors declare no competing financial interest.

■ ACKNOWLEDGMENTS

We acknowledge the facility support of the Molecular Foundry, which was supported by the Office of Science, Office of Basic Energy Sciences, U.S. Department of Energy (DOE), under Contract No. DE-AC02-05CH11231. W.I.L. and Y.H.C. acknowledge funding support from the Ministry of Science and Technology (MOST) in Taiwan (NSC 102-2119-I-009-502). J.X. and X.Z. acknowledge support from the National Basic Research Program of China (2013CB632101) and China Scholarship Council (201406190080). Y.Z. acknowledges support from the China Scholarship Council (201406230186). This project was supported by U.S. DOE Office of Science Early Career Research Program.

■ REFERENCES

(1) Peng, Z.; Yang, H. *Nano Today* **2009**, *4*, 143.

(2) (a) Hao, R.; Xing, R.; Xu, Z.; Hou, Y.; Gao, S.; Sun, S. *Adv. Mater.* **2010**, *22*, 2729. (b) Gu, H.; Xu, K.; Xu, C.; Xu, B. *Chem. Commun.* **2006**, 941.

(3) Frey, N. A.; Peng, S.; Cheng, K.; Sun, S. *Chem. Soc. Rev.* **2009**, *38*, 2532.

(4) (a) Yang, H. *Angew. Chem., Int. Ed.* **2011**, *50*, 2674. (b) Gasteiger, H. A.; Kocha, S. S.; Sompalli, B.; Wagner, F. T. *Appl. Catal., B* **2005**, *56*, 9. (c) Alayoglu, S.; Nilekar, A. U.; Mavrikakis, M.; Eichhorn, B. *Nat. Mater.* **2008**, *7*, 333. (d) Zhang, J.; Lima, F. H. B.; Shao, M. H.; Sasaki, K.; Wang, J. X.; Hanson, J.; Adzic, R. R. *J. Phys. Chem. B* **2005**, *109*, 22701. (e) Mazumder, V.; Chi, M.; More, K. L.; Sun, S. *J. Am. Chem. Soc.* **2010**, *132*, 7848.

(5) Ghosh Chaudhuri, R.; Paria, S. *Chem. Rev.* **2012**, *112*, 2373.

(6) Yin, Y.; Rioux, R. M.; Erdonmez, C. K.; Hughes, S.; Somorjai, G. A.; Alivisatos, A. P. *Science* **2004**, *304*, 711.

(7) Teng, X.; Black, D.; Watkins, N. J.; Gao, Y.; Yang, H. *Nano Lett.* **2003**, *3*, 261.

(8) (a) Zeng, H.; Sun, S.; Li, J.; Wang, Z. L.; Liu, J. P. *Appl. Phys. Lett.* **2004**, *85*, 792. (b) Zeng, H.; Li, J.; Wang, Z. L.; Liu, J. P.; Sun, S. *Nano Lett.* **2004**, *4*, 187.

(9) (a) Yu, Y.; Sun, K.; Tian, Y.; Li, X. Z.; Kramer, M. J.; Sellmyer, D. J.; Shield, J. E.; Sun, S. *Nano Lett.* **2013**, *13*, 4975. (b) Kirkeminde, A.; Ren, S. *Nano Lett.* **2014**, *14*, 4493.

(10) Figuerola, A.; Fiore, A.; Di Corato, R.; Falqui, A.; Giannini, C.; Micotti, E.; Lascialfari, A.; Corti, M.; Cingolani, R.; Pellegrino, T.; Cozzoli, P. D.; Manna, L. *J. Am. Chem. Soc.* **2008**, *130*, 1477.

(11) Liu, C.; Wu, X.; Klemmer, T.; Shukla, N.; Weller, D.; Roy, A. G.; Tanase, M.; Laughlin, D. *Chem. Mater.* **2005**, *17*, 620.

(12) (a) Jungjohann, K. L.; Bliznakov, S.; Sutter, P. W.; Stach, E. A.; Sutter, E. A. *Nano Lett.* **2013**, *13*, 2964. (b) Liao, H.-G.; Cui, L.; Whitelam, S.; Zheng, H. *Science* **2012**, *336*, 1011. (c) Wu, J.; Gao, W.; Wen, J.; Miller, D. J.; Lu, P.; Zuo, J.-M.; Yang, H. *Nano Lett.* **2015**, *15*, 2711.

(13) Liao, H.-G.; Zherebetskyy, D.; Xin, H.; Czarnik, C.; Ercius, P.; Elmlund, H.; Pan, M.; Wang, L.-W.; Zheng, H. *Science* **2014**, *345*, 916.

(14) Yu, Y.; Yang, W.; Sun, X.; Zhu, W.; Li, X. Z.; Sellmyer, D. J.; Sun, S. *Nano Lett.* **2014**, *14*, 2778.

(15) Lifshitz, I. M.; Slyozov, V. V. *J. Phys. Chem. Solids* **1961**, *19*, 35.

(16) (a) Liu, Y.; Tai, K.; Dillon, S. J. *Chem. Mater.* **2013**, *25*, 2927. (b) Bhattacharya, D.; Bosman, M.; Mokkapati, V. R. S. S.; Leong, F. Y.; Mirsaidov, U. *Microsc. Microanal.* **2014**, *20*, 407.

(17) *Nucleation*; Kashchiev, D., Ed.; Butterworth-Heinemann: Oxford, 2000.

(18) (a) Beck, W.; Souza, C. G. S.; Silva, T. L.; Jafelicci, M.; Varanda, L. C. *J. Phys. Chem. C* **2011**, *115*, 10475. (b) Srivastava, C.; Balasubramanian, J.; Turner, C. H.; Wiest, J. M.; Bagaria, H. G.; Thompson, G. B. *J. Appl. Phys.* **2007**, *102*, 104310. (c) Zhang, C.; Wang, H.; Mu, Y.; Zhang, J.; Wang, H. *Nanoscale Res. Lett.* **2014**, *9*, 615.

(19) Shukla, N.; Liu, C.; Jones, P. M.; Weller, D. *J. Magn. Magn. Mater.* **2003**, *266*, 178.

DOI: 10.1021/jacs.5b10076
J. Am. Chem. Soc. 2015, 137, 14850–14853